

# H-MCM-22 沸石分子筛中 Brønsted/Lewis 酸协同效应的<sup>1</sup>H 和 <sup>27</sup>Al 双量子魔角旋转固体核磁共振研究

喻志武<sup>1,2</sup>, 王 强<sup>1</sup>, 陈 雷<sup>1</sup>, 邓 风<sup>1,\*</sup>

<sup>1</sup>中国科学院武汉物理与数学研究所, 波谱与原子分子物理国家重点实验室, 武汉磁共振中心, 湖北武汉 430071

<sup>2</sup>中国科学院强磁场科学中心, 安徽合肥 230031

**摘要:** 采用各种固体核磁共振 (NMR) 技术详细研究了 H-MCM-22 分子筛中 Brønsted/Lewis 酸的协同效应. 二维 <sup>1</sup>H 双量子魔角旋转 (DQ-MAS) NMR 结果表明, 在脱铝 H-MCM-22 分子筛中 Brønsted 酸位 (骨架桥式羟基) 和 Lewis 酸位 (非骨架铝羟基) 之间是空间邻近的, 暗示着可能存在 B/L 酸协同效应. 二维 <sup>27</sup>Al DQ-MAS NMR 结果揭示了各种铝物种之间的空间邻近性, 表明 B/L 酸协同效应优先发生在 H-MCM-22 分子筛超笼中的骨架 T<sub>6</sub> 位铝和非骨架铝物种之间. <sup>13</sup>C-丙酮探针分子实验发现, 因 B/L 酸协同效应而导致脱铝 H-MCM-22 分子筛酸性明显增强, 氘代吡啶探针分子实验也证实在 H-MCM-22 分子筛的超笼中发生了 B/L 酸协同效应. 上述结果将有助于我们理解在脱铝 H-MCM-22 分子筛上发生的多相催化机理.

**关键词:** H-MCM-22 分子筛; 脱铝; 酸性; Brønsted/Lewis 酸协同效应; 双量子魔角旋转核磁共振

中图分类号: O643 文献标识码: A

收稿日期: 2011-07-28. 接受日期: 2011-09-02.

\*通讯联系人. 电话: (027)87198820; 传真: (027)87199291; 电子信箱: dengf@wipm.ac.cn

基金来源: 国家自然科学基金 (20773159, 20933009).

本文的英文电子版(国际版)由Elsevier出版社在ScienceDirect上出版(<http://www.sciencedirect.com/science/journal/18722067>).

## Brønsted/Lewis Acid Sites Synergy in H-MCM-22 Zeolite Studied by <sup>1</sup>H and <sup>27</sup>Al DQ-MAS NMR Spectroscopy

YU Zhiwu<sup>1,2</sup>, WANG Qiang<sup>1</sup>, CHEN Lei<sup>1</sup>, DENG Feng<sup>1,\*</sup>

<sup>1</sup>Wuhan Center for Magnetic Resonance, State Key Laboratory of Magnetic Resonance and Atomic and Molecular Physics, Wuhan Institute of Physics and Mathematics, Chinese Academy of Sciences, Wuhan 430071, Hubei, China

<sup>2</sup>High Magnetic Field Laboratory, Chinese Academy of Sciences, Hefei 230031, Anhui, China

**Abstract:** Brønsted/Lewis acid sites synergy in H-MCM-22 zeolite was studied by solid-state nuclear magnetic resonance (NMR). Two-dimensional <sup>1</sup>H double quantum-magic angle spinning (DQ-MAS) NMR revealed the details of the spatial relationship between the Lewis and the Brønsted acid sites in a dealuminated H-MCM-22 zeolite, which implied the existence of a Brønsted/Lewis acid sites synergy. Two-dimensional <sup>27</sup>Al DQ-MAS NMR was used to give the details of the spatial proximities of various aluminum species. The Brønsted/Lewis acid sites synergy occurred in the supercage of the H-MCM-22 zeolite between a T<sub>6</sub> site Al and extra-framework Al species. <sup>13</sup>C CP/MAS NMR of adsorbed acetone demonstrated that the spatial proximities of the Brønsted and Lewis acid sites led to a synergy that enhanced the Brønsted acid strength of the dealuminated zeolites. <sup>1</sup>H MAS NMR of adsorbed deuterated pyridine confirmed that the Brønsted/Lewis acid sites synergy occurred in the supercage of H-MCM-22. This finding is important for understanding the mechanism of acid-catalyzed reactions on H-MCM-22 zeolites.

**Key words:** H-MCM-22 zeolite; dealumination; acidity; Brønsted/Lewis acid synergy; double quantum-magic angle spinning nuclear magnetic resonance

Received 28 July 2011. Accepted 2 September 2011.

\*Corresponding author. Tel: +86-27-87198820; Fax: +86-27-87199291; E-mail: dengf@wipm.ac.cn

This work was supported by the National Natural Science Foundation of China (20933009, 20773159).

English edition available online at Elsevier ScienceDirect (<http://www.sciencedirect.com/science/journal/18722067>).

沸石分子筛 MCM-22 具有独特的晶体结构 (见图 1)<sup>[1]</sup>, 它同时具有 10 元环和 12 元环的孔道择形效应, 因而广泛应用于众多催化反应<sup>[2–8]</sup>. 众所周知, 当分子筛经过焙烧或者水热处理后, 分子筛骨架发生脱 Al, 形成的非骨架 Al 可作为 Lewis 酸, 极大地改善了分子筛的催化活性和水热稳定性. 与原粉相比, 脱铝后的 H-MCM-22 分子筛在异构化<sup>[3]</sup>、裂解<sup>[6]</sup>、烷基化<sup>[7]</sup>和歧化<sup>[5,8]</sup>等众多多相催化反应中都表现出很高的催化活性和选择性. 以往人们常用 Brønsted 酸和 Lewis 酸协同效应 (或者相互作用) 来解释脱铝分子筛 (例如 Y, ZSM-5 和 MOR 等) 酸催化活性增加的原因<sup>[9–14]</sup>, 但没有直接的实验证据. 因此, 有必要研究 H-MCM-22 分子筛中酸中心的空间邻近性和相互作用来为上述假设提供实验依据.

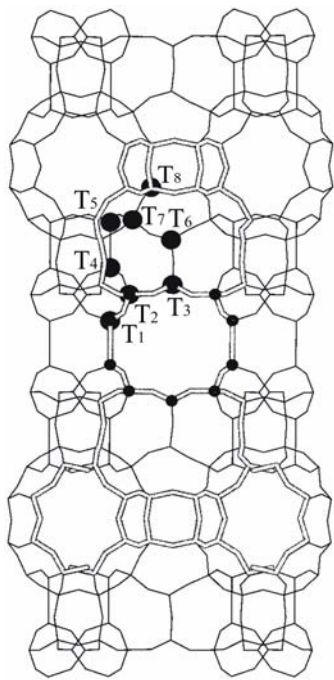


图 1 H-MCM-22 分子筛的结构示意图<sup>[1]</sup>

Fig. 1. Structure of H-MCM-22 zeolite<sup>[1]</sup>.

固体核磁共振波谱 (NMR) 已广泛应用于研究分子筛的表面酸性<sup>[15]</sup>. <sup>1</sup>H 魔角旋转 (MAS) NMR 可以直接给出各种羟基的信息, 如桥式羟基 (SiO–HAl)、硅羟基 (SiOH) 和铝羟基 (AlOH)<sup>[16]</sup>. <sup>29</sup>Si MAS NMR 可以检测分子筛骨架硅铝比以及硅原子周围的局部结构环境. <sup>27</sup>Al 单脉冲 MAS 和多量子 (MQ) MAS 可以用来研究分子筛中骨架铝和非骨架铝物种的含量及配位状态<sup>[17–19]</sup>. 此外, 固体 NMR

结合各种探针分子吸附技术也广泛用来研究分子筛的酸性. 例如, 吸附丙酮的 <sup>13</sup>C CP/MAS NMR 可以用来确定各种固体酸催化剂的酸强度<sup>[20,21]</sup>; 由于三甲基膦 (TMP) 吸附在不同酸位上有较大的化学位移分布, 因而 TMP 探针分子被广泛用来区分酸类型<sup>[22,23]</sup>; 氘代吡啶分子的动力学直径较大 (约 0.7 nm), 采用一些尺寸较小的探针分子 (如丙酮和乙腈), 就能非常容易地揭示酸位的可接近性<sup>[24,25]</sup>. 然而, 上述所有表征手段都不能获得分子筛中各种酸位的空间邻近性以及相互作用的信息.

二维 <sup>1</sup>H 双量子 (DQ) MAS NMR 是研究各种固体材料中质子之间空间邻近性的强有力手段<sup>[26]</sup>. 由于沸石分子筛中各种羟基质子与酸位相关, 因此二维 <sup>1</sup>H DQ-MAS NMR 可以用来研究分子筛中各种酸位之间的空间邻近性. 基于二维 <sup>1</sup>H DQ-MAS NMR 和吸附丙酮探针分子的 <sup>13</sup>C CP/MAS NMR 实验, Li 等<sup>[27,28]</sup>证实了在脱铝 H-Y 分子筛中 B 酸和 L 酸是空间相互邻近的, 而且由于它们之间的协同效应使得脱铝 H-Y 分子筛的酸性明显增强. 类似地, 沸石分子筛中骨架四配位铝物种与分子筛桥式羟基 (Brønsted 酸位) 直接相关, 而非骨架铝物种或三配位骨架铝物种可以作为 Lewis 酸位<sup>[29–32]</sup>, 因此 <sup>27</sup>Al DQ-MAS NMR 也可用来研究分子筛中各种酸位之间的空间邻近性. 最近, Yu 等<sup>[33]</sup>采用灵敏度增强的 <sup>27</sup>Al DQ-MAS NMR 技术揭示了脱铝 H-Y 分子筛中各种铝物种的空间邻近性.

H-MCM-22 分子筛是一种典型的高硅分子筛, 而且其结构独特, 与工业上常用的 Y, ZSM-5, MOR 和 β 等分子筛明显不同, 它存在三种不同的骨架四配位铝物种, 而有关脱铝 H-MCM-22 分子筛中的 B/L 酸协同效应以及各种不等价骨架 T 位之间的空间相关性一直未见文献报道. 本文采用 <sup>27</sup>Al DQ-MAS NMR 和 <sup>1</sup>H DQ-MAS NMR 研究了 H-MCM-22 分子筛中各种铝物种以及各种酸位之间的空间邻近性; 通过丙酮和氘代吡啶探针分子的 NMR 实验, 考察 H-MCM-22 分子筛中 B/L 酸的协同效应. 这些实验结果可能会为理解在 H-MCM-22 分子筛中发生的各种多相酸催化反应机理提供帮助.

## 1 实验部分

### 1.1 催化剂的制备

参照文献[34]合成 MCM-22 分子筛, X 射线衍射 (XRD) 结果显示, 样品中除了 MCM-22 分子筛的衍射峰外, 无其它杂晶信号. 钠型样品在 5%  $\text{O}_2$  气氛下于 810 K 焙烧 48 h 脱除模板剂, 然后在 353 K 用 1 mol/L 的  $\text{NH}_4\text{NO}_3$  溶液交换 4 次. 随后用去离子水洗涤干净, 并在 353 K 干燥过夜, 得到铵交换的  $\text{NH}_4$ -MCM-22 分子筛样品.

为了得到未脱铝的 H-MCM-22 分子筛, 将干燥的  $\text{NH}_4$ -MCM-22 分子筛放在连接有真空系统的玻璃管中从室温升到 373 K, 升温速率 1 K/min, 再以 1.4 K/min 升到 673 K, 然后在真空度为  $1 \times 10^{-3}$  Pa 以下保持 12 h 以上, 最后用氧焰封管保存. 在 H-MCM-22 分子筛的  $^{27}\text{Al}$  MAS NMR 谱中只观察到四配位铝的信号, 表明该法确实能避免加热脱氨过程中脱铝.

将上述合成的  $\text{NH}_4$ -MCM-22 分子筛放置在管式炉石英管中央, 然后从室温以 3 K/min 的升温速率升到 973 K 焙烧 6 h, 即得到脱铝样品. ICP-AES 分析表明, H-MCM-22 分子筛样品脱 Al 前后的 Si/Al 分别为 15 和 20.

## 1.2 固体 NMR 实验

$^1\text{H}$  和  $^{13}\text{C}$  MAS NMR 实验均在 Varian Infinity-plus-400 型波谱仪上进行, 相应的共振频率分别为 400.1 和 100.6 MHz.  $^1\text{H}/^{27}\text{Al}$  TRAPDOR 实验[35]采用 4 mm 的双共振探头采样, 脉冲延迟为 5 s,  $\pi/2$  脉宽设为 2.65  $\mu\text{s}$ , 魔角旋转转速为 10 kHz, 累加 128 次, 对  $^{27}\text{Al}$  的照射时间和射频场强度分别为 200  $\mu\text{s}$  和 65 kHz. 吸附氘代吡啶探针分子的  $^1\text{H}$  MAS NMR 实验采用单脉冲序列采样,  $\pi/2$  脉宽设为 2.65  $\mu\text{s}$ , 魔角旋转转速为 15 kHz, 脉冲延迟为 5 s. 吸附 2- $^{13}\text{C}$ -丙酮的  $^{13}\text{C}$  CP/MAS NMR 实验采用 5 mm 的三共振探头采样,  $^1\text{H} \rightarrow ^{13}\text{C}$  CP/MAS NMR 实验采用六甲苯优化 Hartmann-Hahn 匹配条件, 接触时间设为 5 ms, 脉冲延迟为 5 s, 魔角旋转转速为 8 kHz. 对于  $^1\text{H}$  双量子 NMR 实验, 在准备期用 POST-C7 激发双量子信号, 在混合期则用 POST-C7[36]将双量子信号转化为零量子项. 间接维  $t_1$  增量设置为 20  $\mu\text{s}$ , 直接维和间接维的采样点数分别为 512 和 128 次, 每个  $t_1$  增量都累加 128 次.  $^1\text{H}$  和  $^{13}\text{C}$  的化学位移分别以 TMS 和 HMB 为外标进行定标.

$^{27}\text{Al}$  MAS 和  $^{27}\text{Al}$  DQ-MAS NMR 实验均在

Bruker AVANCE III 800 型波谱仪上进行, 采用 3.2 mm 的 HXY 三共振探头, 实验中  $^{27}\text{Al}$  的共振频率为 208.6 MHz, 样品转速为 21.5 kHz.  $^{27}\text{Al}$  MAS NMR 实验采用小扳倒角的单脉冲序列, 激发  $\pi/12$  脉宽设为 0.5  $\mu\text{s}$ , 脉冲延迟为 1 s. 对于  $^{27}\text{Al}$  DQ-MAS NMR 实验采用 BR2<sub>2</sub> 脉冲序列[37]激发双量子信号, 重耦时间  $\tau_{\text{exc}} = \tau_{\text{rec}} = 1116.30 \mu\text{s}$ , 中心跃迁选择性  $\pi/2$  和  $\pi$  脉宽分别设置为 19 和 38  $\mu\text{s}$ , 每次扫描前都采用 FAM 机制[38]增强信号灵敏度. 间接维转速同步增量设置为 46.51  $\mu\text{s}$ , 直接维和间接维采样点数分别为 400 和 30, 对原粉 H-MCM-22 和脱铝 H-MCM-22 样品直接维每个点数分别累加 13056 和 14080 次, 脉冲延迟为 0.4 s.

## 2 结果与讨论

### 2.1 $^1\text{H}$ MAS 和 $^1\text{H}$ DQ-MAS NMR 结果

$^1\text{H}$  MAS NMR 是研究分子筛中各种表面羟基的强有力手段[39]. 图 2 为 H-MCM-22 分子筛焙烧脱铝前后的  $^1\text{H}$  MAS NMR 谱. 可以看出, H-MCM-22 分子筛原粉主要在  $\delta = 3.8$  和 1.7 处出现两个信号, 可分别归属为桥式羟基 (Brønsted 酸位) 和非酸性的硅羟基[40,41]. 焙烧脱铝处理后, 样品在  $\delta = 2.3$  处出现一个新的共振峰, 可能归属为非骨架 AlOH 或者硅羟基[27,41]. 为了对该信号进行明确归属, 我们用  $^1\text{H}/^{27}\text{Al}$  TRAPDOR 实验[35]研究了脱铝

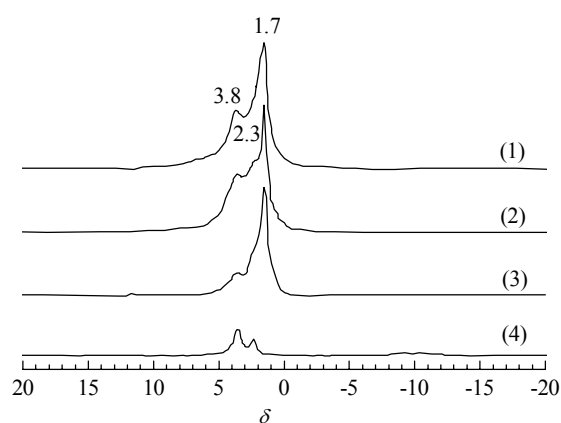


图 2 H-MCM-22 分子筛单脉冲  $^1\text{H}$  NMR 谱以及脱铝 H-MCM-22 分子筛自旋回波 NMR 谱

Fig. 2. The  $^1\text{H}$  single-pulse MAS spectrum of H-MCM-22 (1),  $^1\text{H}$  spin-echo MAS spectra of dealuminated H-MCM-22 without  $^{27}\text{Al}$  irradiation (2) and with  $^{27}\text{Al}$  irradiation (3), and difference spectrum (2)-(3) (4).

H-MCM-22 分子筛中的各种羟基物种. 通过该实验对  $^{27}\text{Al}$  核进行照射后, 和铝物种相关的质子信号强度被明显抑制, 而那些与铝物种不相关的质子的信号强度则不会受影响, 从而可以明确区分羟基物种是否与 Al 物种有关. 可以看出, 当对  $^{27}\text{Al}$  核进行照射后, 位于  $\delta = 2.3$  和  $3.8$  的共振峰强度明显降低, 而位于  $\delta = 1.7$  的峰强度几乎不受影响, 这表明位于  $\delta = 2.3$  的共振峰来自非骨架 AlOH.

分子筛中各种羟基信号与分子筛中酸性质相关联, 因此我们利用  $^1\text{H}$  DQ-MAS NMR 技术研究了分子筛中各种酸位间的空间邻近性<sup>[27,28]</sup>. 由于分子间的偶极相互作用与核间距三次方的倒数成正比, 而  $^1\text{H}$  双量子 NMR 谱峰的信号强度依赖于质子间偶极相互作用的大小, 所以只有质子对的核间距离在  $0.5\text{ nm}$  以内的相关峰才能被观察到. 在两维  $^1\text{H}$  双量子 NMR 图谱中, 自相关峰 ( $\omega, 2\omega$ ) 主要是来自相同化学环境的质子对的自相关, 而位于  $(\omega_a, \omega_a + \omega_b)$  和  $(\omega_b, \omega_a + \omega_b)$  的交叉峰对则是两个不同化学环境的质子对之间的相关峰.

图 3 为 H-MCM-22 分子筛脱铝前后的  $^1\text{H}$  双量子 NMR 谱. 由图可见, 在原粉上出现 2 个自相关峰, 分别位于  $(1.7, 3.4)$  和  $(3.8, 7.6)$  处, 前者表明非酸性的硅羟基彼此之间是空间邻近的, 后者则说明 B 酸位之间也是空间邻近的, 即在高硅 H-MCM-22 分子筛中 B 酸位也不是孤立的而是成对出现的. 焙烧脱铝处理后, H-MCM-22 分子筛的  $^1\text{H}$  双量子谱发生了明显的变化. 首先, 出现了一对明显的交叉峰, 位于  $(2.3, 6.1)$  和  $(3.8, 6.1)$  处, 表明在脱铝 H-MCM-22 分子筛中非骨架铝物种 (Lewis 酸位) 和桥式羟基 (Brønsted 酸位) 之间是空间相互邻近的; 其次, 位于  $(3.8, 7.6)$  的自相关峰强度减弱, 说明脱铝处理导致部分骨架桥式羟基转变成了非骨架铝羟基, 这与  $^1\text{H}$  MAS NMR 结果一致; 最后, 在  $(2.3, 4.6)$  处出现了一个新的自相关峰, 表明脱铝后可能产生了含有两个以上铝羟基的非骨架铝物种, 如  $\text{Al}(\text{OH})_3$  或  $\text{Al}(\text{OH})_2^+$ , 也可能产生了两个相互邻近的  $\text{AlOH}^{2+}$  非骨架铝物种<sup>[27,28]</sup>. 二维  $^1\text{H}$  DQ-MAS NMR 结果表明, H-MCM-22 分子筛中不同酸位间是空间邻近的.

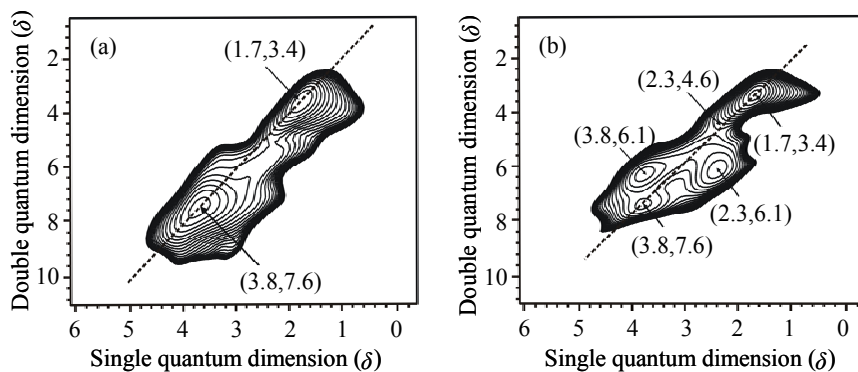


图 3 脱铝前后 H-MCM-22 分子筛的  $^1\text{H}$  DQ-MAS NMR 谱

Fig. 3.  $^1\text{H}$  DQ-MAS NMR spectra of parent H-MCM-22 (a) and dealuminated H-MCM-22 (b).

## 2.2 $^{27}\text{Al}$ MAS 和 $^{27}\text{Al}$ DQ-MAS NMR 结果

分子筛中骨架铝和非骨架铝物种分别起着 B 酸位和 L 酸位的作用, 因而直接影响其催化性能.  $^{27}\text{Al}$  MAS NMR 是研究分子筛中铝物种的配位状态和局部结构的有效手段. 图 4 为高场 ( $18.8\text{ T}$ ) 下 H-MCM-22 分子筛脱铝前后的  $^{27}\text{Al}$  MAS NMR 谱. 可以看出, H-MCM-22 分子筛原粉出现三个共振峰, 分别位于  $\delta = 61, 56$  和  $50$  处, 可归属为四配位骨架铝<sup>[40]</sup>. 焙烧脱铝处理后, 样品于  $\delta = 27$  和  $0$  附近出现了两个宽峰, 并且都呈现出明显的不对称线型, 可

分别归属为五配位和六配位非骨架铝物种<sup>[17–19]</sup>. 结果表明, 高温焙烧可导致 H-MCM-22 分子筛脱铝.

$^{27}\text{Al}$  DQ-MAS NMR 实验技术能够明确揭示各种铝物种之间的空间邻近性. 图 5 为 H-MCM-22 分子筛脱铝前后的  $^{27}\text{Al}$  DQ-MAS NMR 谱. 可以看出, H-MCM-22 分子筛原粉于  $(61, 122), (56, 112)$  和  $(50, 100)$  处出现三组自相关峰, 表明其中三个不等价的四配位骨架铝物种自身之间是彼此空间相互邻近的, 也暗示着骨架桥式羟基 (Brønsted 酸位) 之间也是空间相互邻近的, 这与前文结果一致. 然而, 有

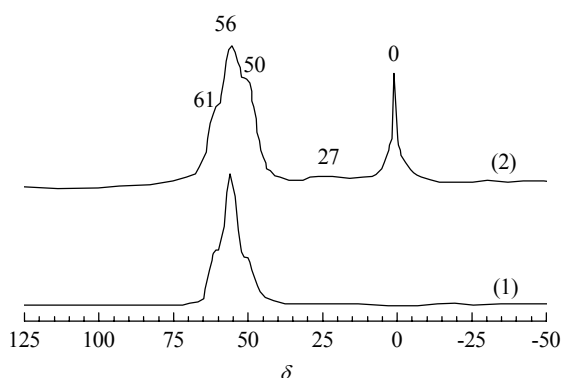


图 4 脱铝前后 H-MCM-22 分子筛的  $^{27}\text{Al}$  MAS NMR 谱  
 Fig. 4.  $^{27}\text{Al}$  MAS NMR spectra of parent H-MCM-22 (1) and dealuminated H-MCM-22 (2).

有趣的是三种骨架铝物种相互之间没有交叉峰, 说明它们彼此之间不是空间相互邻近的. 原粉 H-MCM-22 分子筛焙烧脱铝后的  $^{27}\text{Al}$  DQ-MAS NMR 谱发生了明显的变化. 首先, 位于 (61,122) 的自相关峰消失, 说明脱铝后该不等价骨架四配位铝位彼此之间不再空间相互邻近. 其次, 于 (0,0) 处观察到一个六配位铝物种的自相关峰, 说明该非骨架铝物种自身之间也是彼此空间相互邻近的. 另外, 在位于 (50,50) 和 (0,50) 处观察到了一对重要的交叉峰, 这表明骨架铝物种 (Bronsted 酸位) 与非骨架铝物种 (Lewis 酸位) 之间是空间相互邻近的, 预示着脱铝 H-MCM-22 分子筛中同样可能存在 B/L 酸协同效应. 根据我们前期的  $^{27}\text{Al}$  3Q-MAS NMR 实验及量化计算结果<sup>[42]</sup>, 可将 H-MCM-22 分子筛中三

种不等价 T 位的四配位骨架铝物种进行如下归属: 61 和 50 分别对应于  $T_2$  和  $T_6$  位, 而 56 则对应多个不等价 T 位 ( $T_1, T_3, T_4, T_5, T_7$  和  $T_8$ ) 的无规分布. 根据 H-MCM-22 分子筛的晶体结构以及各种 T 位的归属, 可以推断 B/L 酸协同效应是发生在 H-MCM-22 分子筛的骨架  $T_6$  位和非骨架铝之间, 而  $T_6$  位是位于 MCM-22 分子筛超笼的口袋中. 由此可见, 脱铝 H-MCM-22 分子筛中 B/L 酸协同效应优先发生在超笼的口袋中.

### 2.3 吸附 2- $^{13}\text{C}$ -丙酮的 $^{13}\text{C}$ CP/MAS NMR 结果

2- $^{13}\text{C}$ -丙酮常用作确定固体酸酸强度的探针分子<sup>[20,21]</sup>. 我们前期工作表明, 丙酮羰基碳的  $^{13}\text{C}$  NMR 化学位移值随着酸强度的增强而线性增加,  $\delta = 245$  为超强酸的阈值<sup>[20,21]</sup>. 图 6 是 2- $^{13}\text{C}$ -丙酮吸附在原粉和脱铝 H-MCM-22 分子筛上面的  $^{13}\text{C}$  CP/MAS NMR 谱. 由图可见, H-MCM-22 分子筛原粉于  $\delta = 218$  处出现峰, 可归属为吸附在 B 酸位上没有反应的丙酮. 但在脱铝 H-MCM-22 分子筛上, 于  $\delta = 225, 232$  和  $240$  处出现信号, 其中前两个信号归属为吸附在酸性增强的 B 酸位 (L 酸与 B 酸邻近, 产生协同效应) 上的丙酮分子, 而  $\delta = 240$  处信号则归属为吸附在非骨架铝 (L 酸) 上的丙酮<sup>[27,28]</sup>. 此外, 在脱铝样品上还于  $\delta = 210, 80, 73$  和  $29$  处出现信号, 可归属于丙酮在 H-MCM-22 分子筛上发生二聚或三聚等副反应产物<sup>[43-45]</sup>. 由此可见, 由于存在 B/L 酸协同作用使得脱铝 H-MCM-22 分子筛的酸强度明显增加.

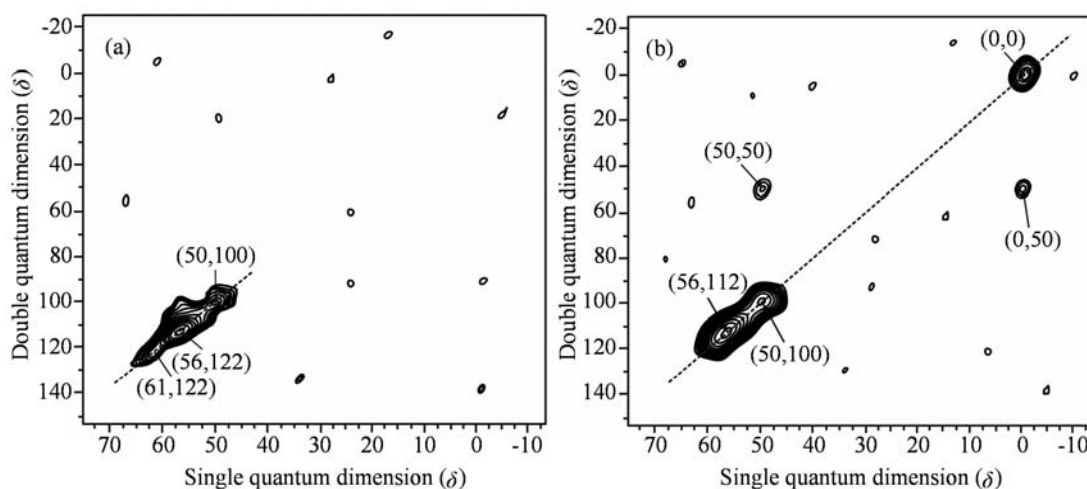


图 5 脱铝前后 H-MCM-22 分子筛的  $^{27}\text{Al}$  DQ-MAS NMR 谱  
 Fig. 5.  $^{27}\text{Al}$  DQ-MAS NMR spectra of parent H-MCM-22 (a) and dealuminated H-MCM-22 (b).

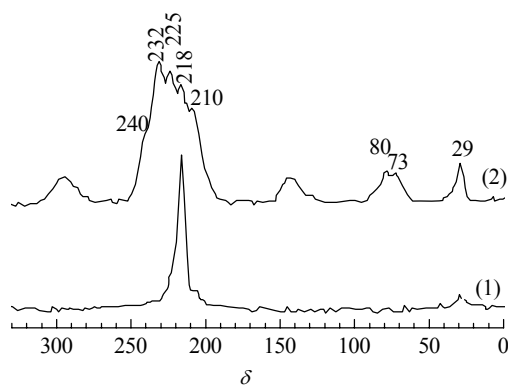


图 6 2-<sup>13</sup>C-丙酮吸附到脱铝前后 H-MCM-22 分子筛上的 <sup>13</sup>C CP/MAS NMR 谱

Fig. 6. <sup>13</sup>C CP/MAS NMR spectra of 2-<sup>13</sup>C-acetone adsorbed on parent H-MCM-22 (1) and dealuminated H-MCM-22 zeolites (2).

#### 2.4 吸附氘代吡啶的 <sup>1</sup>H MAS NMR 结果

氘代吡啶是广泛用作确定固体酸表面各种羟基酸性的探针分子之一<sup>[24,46,47]</sup>。前期工作表明,吡啶吸附在 B 酸位上形成吡啶离子的 <sup>1</sup>H NMR 化学位移可衡量样品的酸强度:即化学位移越小,相应的酸强度越强<sup>[46]</sup>。图 7 为氘代吡啶吸附在脱铝前后的 H-MCM-22 分子筛上的 <sup>1</sup>H MAS NMR 谱。可以看出, H-MCM-22 分子筛原粉于  $\delta = 15.5$  处出现共振峰,可归属为吸附在 B 酸位上的氘代吡啶离子,而在脱铝 H-MCM-22 分子筛上该峰向高场移动至  $\delta = 13.9$  处。因此可以推测,脱铝 H-MCM-22 分子筛中因 B/L 酸协同作用而导致其酸强度明显增加<sup>[27,28,46]</sup>。另据文献报道<sup>[47–50]</sup>,吸附氘代吡啶的 <sup>1</sup>H MAS NMR

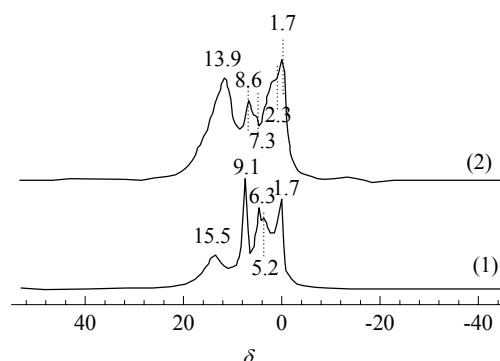


图 7 氘代吡啶吸附到脱铝前后 H-MCM-22 分子筛上的 <sup>1</sup>H MAS NMR 谱

Fig. 7. <sup>1</sup>H MAS NMR spectra of deuterated pyridine adsorbed on parent H-MCM-22 (1) and dealuminated H-MCM-22 zeolites (2).

谱中其它峰的归属如下:对于原粉 H-MCM-22 分子筛,  $\delta = 1.7$  处的峰可归属为不与吡啶发生相互作用的非酸性硅羟基,  $\delta = 5.2, 6.3$  和  $9.1$  的峰可能是由于形成了氢键吡啶所致;对于脱铝 H-MCM-22 分子筛,  $\delta = 2.3$  处共振峰归属为不与氘代吡啶发生相互作用的非骨架铝羟基的信号,  $\delta = 8.6$  和  $7.3$  处峰可归属于吡啶环上的氘原子与酸性质子之间发生 H/D 交换的信号。研究表明, H-MCM-22 分子筛拥有两套独立的孔道结构<sup>[1,34]</sup>:十元环正孔道(平均孔径为  $0.4 \text{ nm} \times 0.59 \text{ nm}$ )和十二元环的半超笼结构(平均孔径为  $0.71 \text{ nm} \times 0.71 \text{ nm} \times 1.81 \text{ nm}$ ),二者之间通过一个孔径为  $0.4 \text{ nm} \times 0.54 \text{ nm}$  的十元环交叉窗口相连。由于氘代吡啶的动力学直径约为  $0.70 \text{ nm}$ ,因此,它不能进入 H-MCM-22 分子筛的十元环孔道中,由此可推测, B/L 酸协同效应将优先发生在 H-MCM-22 分子筛的超笼中,这与前文一致。

### 3 结论

采用二维 <sup>1</sup>H 和 <sup>27</sup>Al DQ-MAS NMR 方法结合探针分子研究了 H-MCM-22 分子筛中 B/L 酸的协同效应。<sup>1</sup>H DQ-MAS NMR 结果表明,脱铝 H-MCM-22 分子筛中 B 酸和 L 酸是相互邻近的,预示着 B/L 酸协同效应可能存在。<sup>27</sup>Al DQ-MAS NMR 结果证实,与 Brønsted 酸位相关的骨架四配位铝物种与非骨架铝物种(Lewis 酸位)也是空间相互邻近的,这也暗示着存在 B/L 酸协同效应。另外,<sup>27</sup>Al DQ-MAS NMR 结果还揭示了 H-MCM-22 分子筛骨架 T<sub>6</sub> 位铝和非骨架铝物种之间产生协同效应,即 B/L 酸协同效应优先发生在超笼的口袋中,与吸附氘代吡啶的 <sup>1</sup>H MAS NMR 结果一致。吸附丙酮的 <sup>13</sup>C CP/MAS 结果则表明因 B/L 酸协同效应而导致 H-MCM-22 分子筛脱铝后的酸强度明显增加。

### 参 考 文 献

- Sastre G, Fornes V, Corma A. *J Phys Chem B*, 2000, **104**: 4349
- Asensi M A, Corma A, Martínez A. *J Catal*, 1996, **158**: 561
- Corma A, Martínez-Triguero J. *J Catal*, 1997, **165**: 102
- Wu P, Komatsu T, Yashima T. *Microporous Mesoporous Mater*, 1998, **22**: 343
- Park S H, Rhee H K. *Appl Catal A*, 2001, **219**: 99
- Okumura K, Hashimoto M, Mimura T, Niwa M. *J Catal*, 2002, **206**: 23

- 7 Fu J Q, Ding C H. *Catal Commun*, 2005, **6**: 770
- 8 Ren X Q, Liang J H, Wang J. *J Porous Mater*, 2006, **13**: 353
- 9 Corma A, Fornes V, Rey F. *Appl Catal*, 1990, **59**: 267
- 10 Lonyi F, Lunsford J H. *J Catal*, 1992, **136**: 566
- 11 Batamack P, Dorémieux-Morin C, Vincent R, Fraissard J. *Microporous Mater*, 1994, **2**: 525
- 12 Viswanadham N, Gupta J K, Dhar G M, Garg M O. *Energy Fuels*, 2006, **20**: 1806
- 13 Kanellopoulos J, Unger A, Schwieger W, Freude D. *J Catal*, 2006, **237**: 416
- 14 Mirodatos C, Barthomeuf D. *J Chem Soc, Chem Commun*, 1981, **2**: 39
- 15 Hunger M. *Catal Rev Sci Eng*, 1997, **39**: 345
- 16 Hunger M. *Solid State Nucl Magn Reson*, 1996, **6**: 1
- 17 Fyfe C A, Bretherton J L, Lam L Y. *J Am Chem Soc*, 2001, **123**: 5285
- 18 Jiao J, Kanellopoulos J, Wang W, Ray S S, Foerster H, Freude D, Hunger M. *Phys Chem Chem Phys*, 2005, **7**: 3221
- 19 van Bokhoven J A, Koningsberger D C, Kunkeler P, van Bekkum H, Kentgens A P M. *J Am Chem Soc*, 2000, **122**: 12842
- 20 Haw J F, Nicholas J B, Xu T, Beck L W, Ferguson D B. *Acc Chem Res*, 1996, **29**: 259
- 21 Fang H J, Zheng A M, Chu Y Y, Deng F. *J Phys Chem C*, 2010, **114**: 12711
- 22 Lunsford J H, Rothwell W P, Shen W. *J Am Chem Soc*, 1985, **107**: 1540
- 23 Kao H M, Grey C P. *Chem Phys Lett*, 1996, **259**: 459
- 24 Hung J, Jiang Y J, Marthala V R R, Thomas B J, Romanova E, Hunger M. *J Phys Chem C*, 2008, **112**: 3811
- 25 Freude D, Hunger M, Pfeifer H, Schwieger W. *Chem Phys Lett*, 1986, **128**: 62
- 26 Brown S P, Spiess H W. *Chem Rev*, 2001, **101**: 4125
- 27 Li S H, Zheng A M, Su Y C, Zhang H L, Chen L, Yang J, Ye C H, Deng F. *J Am Chem Soc*, 2007, **129**: 11161
- 28 Li S H, Huang S J, Shen W L, Zhang H L, Fang H J, Zheng A M, Liu S B, Deng F. *J Phys Chem C*, 2008, **112**: 14486
- 29 Mota C J A, Bhering D L, Rosenbach N. *Angew Chem, Int Ed*, 2004, **43**: 3050
- 30 Carvajal R, Chu P, Lunsford J H. *J Catal*, 1990, **125**: 123
- 31 Sokol A A, Catlow C R A, Garces J M, Kuperman A. *Adv Mater*, 2000, **12**: 1801
- 32 van Bokhoven J A, van der Eerden A M J, Koningsberger D C. *J Am Chem Soc*, 2003, **125**: 7435
- 33 Yu Z W, Zheng A M, Wang Q, Chen L, Xu J, Amoureux J P, Deng F. *Angew Chem, Int Ed*, 2010, **49**: 8657
- 34 Leonowicz M E, Lawton J A, Lawton S L, Rubin M K. *Science*, 1994, **264**: 1910
- 35 Grey C P, Vega A J. *J Am Chem Soc*, 1995, **117**: 8232
- 36 Hohwy M, Jakobsen H J, Eden M, Levitt M H, Nielsen N C. *J Chem Phys*, 1998, **108**: 2686
- 37 Wang Q, Hu B W, Lafon O, Trébosc J, Deng F, Amoureux J P. *J Magn Reson*, 2009, **200**: 251
- 38 Madhu P K, Goldbourt A, Frydman L, Vega S. *Chem Phys Lett*, 1999, **307**: 41
- 39 Mastikhin V M, Mudrakovsky I L, Nosov A V. *Progr Nucl Magn Reson Spectrosc*, 1991, **23**: 259
- 40 Ma D, Han X W, Xie S J, Bao X H, Hu B, Au-Yeung S C F. *Chem Eur J*, 2002, **8**: 162
- 41 Ma D, Deng F, Fu R Q, Han X W, Bao X H. *J Phys Chem B*, 2001, **105**: 1770
- 42 陈雷, 邓风, 叶朝辉. 物理化学学报 (Chen L, Deng F, Ye Ch H. *Acta Phys-Chim Sin*), 2003, **19**: 805
- 43 Xu T, Kob N, Drago R S, Nicholas J B, Haw J F. *J Am Chem Soc*, 1997, **119**: 12231
- 44 Xu T, Haw J F. *J Am Chem Soc*, 1994, **116**: 10188
- 45 Biaglow A I, Sepa J, Gorte R J, White D. *J Catal*, 1995, **151**: 373
- 46 Zheng A M, Zhang H L, Chen L, Yue Y, Ye Ch H, Deng F. *J Phys Chem B*, 2007, **111**: 3085
- 47 Yu H G, Fang H J, Zhang H L, Li B J, Deng F. *Catal Commun*, 2009, **10**: 920
- 48 Xu J, Zheng A M, Yang J, Su Y C, Wang J Q, Zeng D L, Zhang M J, Ye Ch H, Deng F. *J Phys Chem B*, 2006, **110**: 10662
- 49 胡伟, 罗晴, 李申慧, 申万岭, 岳勇, 邓风. 物理化学学报 (Hu W, Luo Q, Li Sh H, Shen W L, Yue Y, Deng F. *Acta Phys-Chim Sin*), 2006, **22**: 1233
- 50 Freude D. *Chem Phys Lett*, 1995, **235**: 69

## 英 译 文

### *English Text*

The zeolite MCM-22 has a unique crystalline structure (see Fig. 1) [1] that combines both the 10 member ring (MR) and 12 MR systems, and much attention has been paid to its catalytic reactions [2–8]. As is well-known, a hydrothermal or calcination treatment of a zeolite usually causes the dealumination of its framework, which forms extra-framework aluminium (EFAL) species that can considerably enhance the catalytic activity of the zeolite. As compared with the parent H-MCM-22 zeolite, dealuminated H-MCM-22 zeolite has exhibited much higher activity and selectivity in many heterogeneous catalytic reactions, such as isomerization [3], cracking [6], alkylation [7], and disproportionation [5,8]. Although there has been no direct experimental evidence, many researchers have suggested a Brønsted/Lewis acid sites synergy (or interaction) to interpret the high catalytic activity of dealuminated zeolites (Y, ZSM-5, MOR, etc.) [9–14]. As such, it is desirable to explore the spatial relationships and interactions between various acid sites to provide direct experimental evidence for a Brønsted/Lewis acid sites synergy in dealuminated H-MCM-22 zeolites.

Solid-state nuclear magnetic resonance (NMR) spectroscopy has been widely applied to the study of the acidity of zeolites [15].  $^1\text{H}$  magic angle spinning (MAS) NMR can give direct information on the various hydroxyl groups, SiOHAl, AlOH, and SiOH groups, in zeolites [16].  $^{29}\text{Si}$  MAS NMR

can give information on the Si/Al ratio of the zeolite framework and the local structural environment around  $^{29}\text{Si}$  atoms.  $^{27}\text{Al}$  single pulse MAS and multiple-quantum (MQ) MAS NMR techniques can be employed to determine the coordination and concentration of both framework Al and EFAL species in zeolites [17–19]. Moreover, solid-state NMR combined with probe molecules has been widely used to study the acidity of zeolites, e.g.,  $^{13}\text{C}$  MAS NMR of adsorbed 2- $^{13}\text{C}$ -acetone had been used to measure the relative acid strengths of various solid catalysts [20,21], and  $^{31}\text{P}$  NMR of trimethylphosphine (TMP) bound to different acid sites has a large chemical shift range, thus, it has been used to easily distinguish Brønsted and Lewis acid sites [22,23]. Deuterated pyridine with a molecular size of about 0.7 nm can be used to probe the accessibility [24,25] of the acid sites in zeolites by using it together with smaller probe molecules such as acetone and deuterated acetonitrile. However, these experimental techniques are unable to provide information about the spatial relationships or interactions between various acid sites in zeolites.

Two-dimensional  $^1\text{H}$  double quantum (DQ) MAS NMR is a useful method for probing proton-proton proximities in various solid materials [26].  $^1\text{H}$  NMR signals can distinguish between various hydroxyl groups that act as different acid sites, and  $^1\text{H}$  DQ-MAS NMR has been employed to investigate the spatial proximities of the various acid sites in dealuminated zeolites. On the basis of  $^1\text{H}$  DQ-MAS NMR and the  $^{13}\text{C}$  MAS NMR of adsorbed 2- $^{13}\text{C}$ -acetone, we have obtained the spatial details of the Brønsted and Lewis acid sites in a dealuminated H-Y zeolite and demonstrated that spatial proximities can result in a synergy effect that remarkably increases the acid strength of the zeolite [27,28]. In zeolites, Brønsted acid sites are due to bridging hydroxyl groups (SiOHAl) and a 4-coordinate framework aluminum, while Lewis acid sites are due to either EFAL [29,30] or three-coordinate framework aluminum species [31,32]. Recently, we have used  $^{27}\text{Al}$  DQ-MAS NMR spectroscopy to reveal the detailed spatial proximities of the various aluminum species in dealuminated H-Y zeolites [33].

H-MCM-22 is a typical highly siliceous zeolite and possesses a unique crystalline structure and three types of framework aluminum species, so it is quite different from other industrially important zeolites such as Y, ZSM-5, MOR, and  $\beta$ . Unfortunately, up to now, there had been no information on the Brønsted/Lewis acid sites synergy effect and the spatial proximities of the various nonequivalent T positions in H-MCM-22 zeolite. In this work, we explored the spatial proximities of various acid sites and aluminum species in H-MCM-22 by two-dimensional  $^1\text{H}$  and  $^{27}\text{Al}$  2D DQ-MAS NMR techniques in conjunction with one-dimensional  $^1\text{H}$  and  $^{27}\text{Al}$  MAS NMR spectroscopy. The  $^{13}\text{C}$  CP/MAS NMR result from adsorbed acetone demonstrated that the spatial

proximities between Brønsted and Lewis acid sites lead to a synergy effect that remarkably enhanced the Brønsted acid strength of the dealuminated zeolites. The  $^1\text{H}$  MAS NMR result of adsorbed deuterated pyridine confirmed that the Brønsted/Lewis acid sites synergy occurred in the supercage of H-MCM-22. These findings are important for understanding the mechanism of acid-catalyzed reactions occurring in H-MCM-22.

## 1 Experimental

### 1.1 Catalyst preparation

MCM-22 was synthesized by a preparation method reported in the literature [34]. XRD data showed that the MCM-22 zeolite had the typical MCM-22 crystalline structure, and no peak of any other crystalline structure was observed. To remove the template, the synthesized solid was calcined for 48 h at 810 K under nitrogen containing 5 vol% oxygen. The ammonium form was prepared by four times ion exchange at 350 K with 1 mol/L  $\text{NH}_4\text{NO}_3$ . The resulting  $\text{NH}_4$ -MCM-22 zeolite was first dried overnight in air at 353 K and then dehydrated under vacuum ( $< 10^{-5}$  Pa). To avoid dealumination of the zeolite during dehydration, the temperature was first increased from room temperature to 373 K at a rate of 1 K/min, then from 373 to 673 K at a rate of 1.4 K/min, and then kept at 673 K for 12 h. Finally, the H-MCM-22 zeolite was obtained. It was shown by  $^{27}\text{Al}$  MAS NMR that there was no extraframework Al in the H-MCM-22 zeolite.

Dealuminated H-MCM-22 zeolite was prepared as follows. The  $\text{NH}_4$ -MCM-22 sample was placed in a quartz crucible in a tube furnace and calcined at 973 K in air for 6 h with the temperature raised from room temperature to 973 K at a rate of 3 K/min. ICP-AES analysis showed that the Si/Al ratios of the parent and dealuminated H-MCM-22 were 15 and 20, respectively.

### 1.2 Solid-state NMR measurements

$^1\text{H}$  and  $^{13}\text{C}$  MAS NMR experiments, respectively, were performed on a Varian Infinity-plus 400 spectrometer at the resonance frequencies of 400.1 and 100.6 MHz.  $^1\text{H}/^{27}\text{Al}$  transfer of population in double resonance (TRAPDOR) experiments [35] were carried out with a 4 mm MAS probe at a spinning rate of 10 kHz, and the data were acquired with a  $\pi/2$  pulse length of 2.65  $\mu\text{s}$ , a recycle delay of 5 s, and 128 accumulations. An irradiation time of 200  $\mu\text{s}$  (two rotor periods) and a radio frequency field strength of 65 kHz for the  $^{27}\text{Al}$  nuclei were used.  $^1\text{H}$  MAS NMR spectra of adsorbed deuterated pyridine (pyridine- $d_5$ ) were recorded using a single pulse sequence with a  $\pi/2$  pulse length of 2.65  $\mu\text{s}$ , a

spinning rate of 15 kHz, and a 5 s recycle delay.  $^1\text{H}\rightarrow^{13}\text{C}$  CP/MAS NMR experiments of adsorbed  $2\text{-}^{13}\text{C}$ -acetone were performed with a 5 mm probe, and the Hartmann-Hahn condition was optimized by using hexamethylbenzene (HMB) with a contact time of 5 ms, a recycle delay of 4 s, and a sample spinning rate of 8 kHz.  $^1\text{H}$  DQ-MAS NMR spectra were obtained with a 4 mm MAS probe with a sample spinning rate of 14.286 kHz. DQ coherences were excited and reconverted with the POST-C7 [36] pulse sequence by the general scheme used in two-dimensional multiple-quantum spectroscopy. The increment in the indirect dimension ( $t_1$ ) was set to 17.5  $\mu\text{s}$ . 256 scans were acquired for each  $t_1$  increment and two-dimensional data sets consisted of  $128 t_1 \times 512 t_2$ . The chemical shifts of  $^1\text{H}$  and  $^{13}\text{C}$  were referenced to TMS and HMB, respectively.

$^{27}\text{Al}$  MAS and DQ-MAS NMR experiments were carried out on a Bruker AVANCE III 800 spectrometer at a resonance frequency of 208.6 MHz using a 3.2 mm HXY triple-resonance MAS probe at a sample spinning rate of 21.5 kHz.  $^{27}\text{Al}$  MAS NMR spectra were recorded by the small flip angle technique with a pulse length of 0.5  $\mu\text{s}$  ( $< \pi/12$ ) and a recycle delay of 1 s. A CT-selective  $\pi/2$  pulse of 19  $\mu\text{s}$  and  $\pi$  pulse of 38  $\mu\text{s}$  were used for the  $^{27}\text{Al}$  DQ-MAS experiments and the signal sensitivity was enhanced by initiating each transient by the FAM scheme [37]. DQ coherences were excited and reconverted using a BR2<sub>1</sub> pulse sequence [38] with  $\tau_{\text{exc}} = \tau_{\text{rec}} = 1116.30 \mu\text{s}$  by the general scheme used in 2D multiple-quantum spectroscopy of dipolar-coupled quadrupolar spins. The rotor-synchronized increment interval in the indirect dimension was set to 46.51  $\mu\text{s}$  and the two-dimensional data sets consisted of  $30 t_1 \times 400 t_2$  points. 13056 and 14080 FIDs, respectively, were acquired for each  $t_1$  increment using a recycle delay of 0.4 s for obtaining the 2D  $^{27}\text{Al}$  DQ spectra of the parent and dealuminated H-MCM-22 samples.

## 2 Results and discussion

### 2.1 $^1\text{H}$ MAS and DQ-MAS NMR

Solid-state  $^1\text{H}$  MAS NMR is a powerful tool for identifying the different surface OH groups in zeolites [39]. Figure 2 shows the  $^1\text{H}$  MAS spectra of the H-MCM-22 zeolite before and after calcination. With the parent H-MCM-22 (Fig. 2(1)), only two main peaks at  $\delta = 3.8$  and 1.7 were resolved clearly, which were, respectively, assigned to bridging SiOHAl groups (Brønsted acid site) and silanol groups [40,41]. After calcination, a new signal at  $\delta = 2.3$  was observed in the dealuminated H-MCM-22 zeolite, which could be due to an extra-framework AlOH species or another kind of silanol group [27,41]. To determine this, we performed  $^1\text{H}/^{27}\text{Al}$  TRAPDOR experiments [35] on the dealuminated

H-MCM-22 zeolite. This method can distinguish between OH species with and without a connection to an Al atom. Under  $^{27}\text{Al}$  irradiation, the signals of protons that are strongly coupled to aluminum atoms will be significantly suppressed, while those from protons that are not coupled to aluminum atoms will remain unaffected. As shown in the spectra of the dealuminated H-MCM-22 (Fig. 2(3) and (4)), after Al irradiation, the lines at  $\delta = 3.8$  and 2.3 were suppressed, while the peak at  $\delta = 1.7$  remained unchanged. The results confirmed that the shoulder at  $\delta = 2.3$  was due to hydroxyl protons associated with EFAL species.

Because the  $^1\text{H}$  NMR signals of H-MCM-22 are due to various hydroxyl groups that can act as different types of acid sites,  $^1\text{H}$  DQ-MAS NMR can be employed to investigate the spatial neighbors of the various acid sites [27,28]. The presence of a signal in the  $^1\text{H}$  DQ-MAS spectrum indicated that two protons were in close proximity ( $< 0.5 \text{ nm}$ ) because the DQ coherences observed were strongly dependent on the internuclear distance. The peaks that occurred along the diagonal ( $\omega, 2\omega$ ) were autocorrelation peaks resulting from the dipolar interaction of protons with the same chemical shift, while pairs of off-diagonal peaks at ( $\omega_a, \omega_a + \omega_b$ ) and ( $\omega_b, \omega_a + \omega_b$ ) were due to two protons with different chemical shifts.

Figure 3(a) shows the  $^1\text{H}$  DQ-MAS NMR spectrum of the parent H-MCM-22 zeolite. The appearance of two autocorrelation peaks at  $\delta = (1.7, 3.4)$  and  $(3.8, 7.6)$  indicated that both bridging hydroxyl groups (SiOHAl, Brønsted acid site) and non-acidic silanols were in close proximity to each other. Upon dealumination of the zeolite by calcination, notable changes in the  $^1\text{H}$  DQ-MAS NMR spectra occurred, as shown in Fig. 3(b). First, one cross-peak pair at  $\delta = (2.3, 6.1)$  and  $(3.8, 6.1)$  appeared, which was due to correlations between adjacent pairs of extra-framework AlOH (Lewis acid sites) and bridging hydroxyl groups (Brønsted acid sites). Second, the signal intensity of the autocorrelation peak at  $\delta = (3.8, 7.6)$  decreased, suggesting that some bridging hydroxyls (SiOHAl) were converted to EFAL species by the calcination treatment, which agreed with the  $^1\text{H}$  MAS NMR spectra. Third, a new autocorrelation peak at  $\delta = (2.3, 4.6)$  appeared, which was due to extra-framework AlOH<sup>2+</sup> in close proximity or EFAL species with more than one hydroxyl groups such as Al(OH)<sub>3</sub> and Al(OH)<sub>2</sub><sup>+</sup> [27,28]. Clearly, the two-dimensional  $^1\text{H}$  DQ-MAS NMR experiments were capable of revealing the detailed spatial proximities of the various acid sites in H-MCM-22.

### 2.2 $^{27}\text{Al}$ MAS and $^{27}\text{Al}$ DQ-MAS NMR

As is well-known, framework and extra-framework aluminum acting as Brønsted and Lewis acids, respectively, play key roles in catalytic reactions.  $^{27}\text{Al}$  MAS NMR has

been used to determine the coordination and local structure of specific aluminium species in zeolites. The  $^{27}\text{Al}$  MAS NMR (18.8 T) spectra of H-MCM-22 before and after calcination are shown in Fig. 4. Three groups of peaks at  $\delta = 61$ , 56, and 50 were observed in the parent H-MCM-22 zeolite. All of these were assigned to four-coordinate framework Al [40]. After the dealumination treatment, two more broad peaks at ca.  $\delta = 27$  and 0, which were due to five- and six-coordinate EFAL species [17–19], appeared at the expense of the four-coordinate framework aluminum. Both of these had an unsymmetrical line shape.

The two-dimensional  $^{27}\text{Al}$  DQ-MAS NMR experiment is a useful method for probing aluminum-aluminum proximities. To identify the spatial proximity and interaction of various aluminum species, a sensitivity-enhanced  $^{27}\text{Al}$  DQ-MAS NMR technique [38] at high field (18.8 T) was applied to the parent and dealuminated H-MCM-22 zeolites. Figure 5(a) displays the  $^{27}\text{Al}$  DQ-MAS NMR spectrum of the parent H-MCM-22 zeolite. Three autocorrelation peaks at  $\delta = (61,122)$ ,  $(56,112)$ , and  $(50,100)$  can be clearly distinguished. These indicated that the four-coordinate framework Al species, which are associated with bridging hydroxyl groups (SiOHAl, Brønsted acid site), were in close proximity to one another. This is in agreement with the above  $^1\text{H}$  DQ-MAS results. However, it is interesting to note that the three kinds of framework Al species were not in close proximity to one another because of the absence of any cross-peak among them. Upon dealumination of the zeolite by calcination, the  $^{27}\text{Al}$  DQ-MAS NMR spectrum changed dramatically (Fig. 5(b)). First, the autocorrelation peak at  $\delta = (61,122)$  disappeared, suggesting that the nonequivalent four-coordinate framework Al species were no longer in close proximity to each other, which is in good agreement with the observation that the signal intensity of the bridging hydroxyls (SiOHAl) autocorrelation peak decreased in the  $^1\text{H}$  DQ-MAS NMR spectrum of the dealuminated H-MCM-22. Second, a new autocorrelation peak at  $\delta = (0,0)$  appeared, indicating that the six-coordinate EFAL species were in close proximity to each other. Finally, a very important cross-peak pair between the four-coordinate framework Al and six-coordinate EFAL ( $\delta = (50,50)$ ,  $(0,50)$ ) appeared. This indicated that the four-coordinate framework Al associated with Brønsted acid site (SiOHAl) was in close proximity to the six-coordinate EFAL species, resulting from the dealumination, which acts as a Lewis acid site in zeolites. In our previous studies [42], on the basis of  $^{27}\text{Al}$  3Q MAS NMR results and DFT calculations, we had distinguished three kinds of nonequivalent T positions: the resonance at  $\delta = 61$  was assigned to the  $T_2$  site, the  $\delta = 50$  was assigned to the  $T_6$  site, but the  $\delta = 56$  corresponded to the random distribution of many nonequivalent T positions. From the crystalline structure and the assignment of the

various T positions in H-MCM-22 zeolite, we can conclude that the Brønsted/Lewis acid synergy occurred in the supercage of H-MCM-22 between a  $T_6$  site framework Al and an extra-framework Al species.

### 2.3 $^{13}\text{C}$ CP/MAS NMR of adsorbed 2- $^{13}\text{C}$ -acetone

2- $^{13}\text{C}$ -acetone is a well-established NMR probe molecule for evaluating the relative acid strengths of solid acids [20,21]. Recently, we have established a linear correlation between the  $^{13}\text{C}$  isotropic chemical shift of adsorbed acetone and Brønsted acid strength with the aid of DFT calculations [21]. A stronger Brønsted acidity gives a larger  $^{13}\text{C}$  isotropic chemical shift. The threshold acid strength of a solid superacid gives rise to an isotropic  $^{13}\text{C}$  NMR chemical shift of resonance at  $\delta = 245$  from adsorbed 2- $^{13}\text{C}$ -acetone [20,21]. Figure 6 shows the  $^{13}\text{C}$  CP/MAS NMR spectra of 2- $^{13}\text{C}$ -acetone (0.2 mmol/g) adsorbed on the parent and dealuminated H-MCM-22 zeolites. For the parent H-MCM-22 zeolite, only one sharp resonance at  $\delta = 218$  due to unreacted acetone adsorbed on the Brønsted acid site of H-MCM-22 was observed. However, for the dealuminated H-MCM-22 zeolite, three additional resonances were observed at  $\delta = 225$ , 232, and 240. From our previous work [27,28], the peaks at  $\delta = 225$  and 232 were assigned to acetone adsorbed on Brønsted acid sites of stronger acid strength (than the site associated with the peak at  $\delta = 218$ ) that were interacting with Lewis acid sites, while the shoulder peak at  $\delta = 240$  is likely associated with acetone directly adsorbed on Lewis acid sites. In addition, the other resonance signals at  $\delta = 210$ , 80, 73, and 29 can be attributed to the products formed from the aldol reaction of acetone [43–45]. Therefore, the  $^{13}\text{C}$  NMR results of adsorbed acetone confirmed the presence of a Brønsted/Lewis acid synergy effect in the dealuminated H-MCM-22 zeolite.

### 2.4 $^1\text{H}$ MAS NMR of adsorbed deuterated pyridine

Ppyridine- $d_5$  is a probe molecule widely used for the determination of the acid property of surface OH groups [24,46,47]. Our previous work indicated that the  $^1\text{H}$  chemical shift of pyridinium ions can be used to measure the acid strength: a smaller chemical shift corresponded to a stronger acid strength [46]. Figure 7 displays the  $^1\text{H}$  MAS NMR spectra of pyridine- $d_5$  adsorbed on the parent and dealuminated H-MCM-22 zeolites. In the adsorption of pyridine- $d_5$  on the parent H-MCM-22 zeolite, the peak at  $\delta = 15.5$  can be assigned to pyridine- $d_5$  molecules adsorbed on Brønsted acid sites. However, after the adsorption of pyridine- $d_5$  on the dealuminated H-MCM-22 zeolite, this signal moved to higher field and appeared at  $\delta = 13.9$ . From our previous works [27,28,46], we can conclude that the acid strength of

the corresponding Brønsted acid site, compared with that of the parent H-MCM-22 zeolite, was remarkably enhanced because of the Brønsted/Lewis acid sites synergy. The signals at  $\delta = 1.7$  and  $2.3$  in the  $^1\text{H}$  MAS spectra of pyridine- $\text{d}_5$ -loaded H-MCM-22 zeolite were probably due to unreacted SiOH and AlOH, respectively. The signals at  $\delta = 5.2$ ,  $6.3$ , and  $9.1$  implied that hydrogen-bonded pyridine was probably formed [47–49]. However, the signals at  $\delta = 8.6$  and  $7.3$  were probably due to H/D exchange between the deuterons in the ring of pyridine and the acidic proton [50]. The H-MCM-22 zeolite possesses two independent microporous systems [1,34]: one has sinusoidal channels consisting of 10-MR, with an average dimension of  $0.4 \text{ nm} \times 0.59 \text{ nm}$ , and the other has larger supercages ( $0.71 \text{ nm} \times 0.71 \text{ nm} \times 1.81 \text{ nm}$ ) composed of 12-MR that are interconnected by 10-MR windows ( $0.4 \text{ nm} \times 0.54 \text{ nm}$ ). The molecular size of pyridine- $\text{d}_5$  is such that it is too large (kinetic diameter is  $0.70 \text{ nm}$ ) and cannot enter the 10-MR channels, so it was concluded that the Brønsted/Lewis acid sites synergy effect was in the supercage of the H-MCM-22 zeolite. The  $^1\text{H}$  MAS NMR results of adsorbed deuterated pyridine are in agreement with the  $^{27}\text{Al}$  DQ-MAS NMR experiments described above.

### 3 Conclusions

Brønsted/Lewis acid sites synergy and the spatial proximities of the acid sites in H-MCM-22 were investigated by  $^1\text{H}$  and  $^{27}\text{Al}$  DQ-MAS NMR. Both  $^1\text{H}$  and  $^{27}\text{Al}$  DQ-MAS NMR results revealed that the Lewis acid sites were in close proximity to the Brønsted acid sites, implying the existence of a Brønsted/Lewis acid sites synergy in dealuminated H-MCM-22 zeolites. The  $^{27}\text{Al}$  DQ-MAS NMR results demonstrated that the Brønsted/Lewis acid sites synergy occurred between a  $\text{T}_6$  framework Al site and an extra-framework Al species.  $^{13}\text{C}$  CP/MAS NMR of adsorbed 2- $^{13}\text{C}$ -acetone showed a remarkable increase in the acid strength of the dealuminated H-MCM-22 zeolite due to the existence of the Brønsted/Lewis acid sites synergy.  $^1\text{H}$  MAS NMR of adsorbed pyridine- $\text{d}_5$  also confirmed that the Brønsted/Lewis acid sites synergy occurred in the supercage of H-MCM-22. These findings are important for understanding the mechanism of acid-catalyzed reactions in H-MCM-22 zeolites.

*Full-text paper available online at Elsevier ScienceDirect*  
<http://www.sciencedirect.com/science/journal/18722067>